PNAS RESEARCH ARTICLE | APPLIED PHYSICAL SCIENCES
BIOPHYSICS AND COMPUTATIONAL BIOLOGY

Bimodal brush-functionalized nanoparticles selective to receptor surface density

Huu Trong Phan[a], Dominic Lauzon[b], Alexis Vallée-Bélisle[b], Stefano Angioletti-Uberti[c], Jeanne Leblond Chain[a,d,1], and Suzanne Giasson[a,b,1]

Edited by David Weitz, Harvard University, Cambridge, MA; received May 15, 2022; accepted November 25, 2022

Nanoparticles or drug carriers which can selectively bind to cells expressing receptors above a certain threshold surface density are very promising for targeting cells overexpressing specific receptors under pathological conditions. Simulations and theoretical studies have suggested that such selectivity can be enhanced by functionalizing nanoparticles with a bimodal polymer monolayer (BM) containing shorter ligated chains and longer inert protective chains. However, a systematic study of the effect of these parameters under tightly controlled conditions is still missing. Here, we develop well-defined and highly specific platforms mimicking particle–cell interface using surface chemistry to provide a experimental proof of such selectivity. Using surface plasmon resonance and atomic force microscopy, we report the selective adsorption of BM-functionalized nanoparticles, and especially, a significant enhanced selective behavior by using a BM with longer protective chains. Furthermore, a model is also developed to describe the repulsive contribution of the protective brush to nanoparticle adsorption. This model is combined with super-selectivity theory to support experimental findings and shows that the observed selectivity is due to the steric energy barrier which requires a high number of ligand–receptor bonds to allow nanoparticle adsorption. Finally, the results show how the relative length and molar ratio of two chains can be tuned to target a threshold surface density of receptors and thus lay the foundation for the rational design of BM-functionalized nanoparticles for selective targeting.

bimodal brush | functionalization | receptor surface density | selectivity | nanoparticle

Significance

This work provides the detailed experimental evidence of recent simulations showing that the selectivity of nanoparticle–cell interactions can be improved by introducing an extra steric repulsion provided by a protective polymer brush shielding ligands. The repulsion contribution is experimentally tuned by adjusting the surface density and molecular weight of the protective polymer. This repulsion makes the nanoparticle adsorption more selective to the variation in receptor surface density. Our study suggests a way to facilitate the design of supramolecular constructs that exhibit desired super-selectivity to surface density of receptors.

Engineering of drug delivery vehicles that selectively target affected cells while ignoring healthy ones has been a primary goal and remains a challenging task in nanomedicine (1). Multivalent nanoparticles, nanoparticles being surface-functionalized with several identical ligands attached to flexible and inert linkers (called ligated chains), are engineered to target cell surfaces overexpressing a specific receptor (2). The multivalent interactions between such functionalized nanoparticles and cell surfaces expressing a specific type of receptor are mediated by the simultaneous binding of several ligands (of the same type) to several receptors (of the same type) (3). Such multivalent interactions play a critical role in numerous biological processes (3, 4) and in the fate of nanomedicines in biological media (2, 5) thanks to their super-selectivity (3, 6). Super-selectivity is defined as the supralinear growth in nanoparticle adsorption as a function of receptor surface density (7). Such dependence to receptor surface density is indeed highly beneficial to selective targeting of cell surfaces expressing receptors above a given threshold surface density. The theoretical rationale for the super-selectivity of multivalent nanoparticles is that the number of possible ligand–receptor binding arrangements increases in a highly nonlinear manner with the receptor surface density due to combinatorial entropy (7, 8). Interestingly, a previously reported statistical mechanical description of this phenomenon shows that the super-selectivity is enhanced when the ligand–receptor affinity decreases (7, 9–11). The results have been validated by experimental data (11–15), Monte Carlos simulations (9, 16, 17), and other theoretical studies (8, 10, 13, 16, 18–20), which fostered multivalent nanoparticles for the development of targeted drug delivery (2, 21).

Recent theoretical works have demonstrated that the super-selectivity can be enhanced by coating multivalent nanoparticles with a bimodal polymer monolayer (BM) with shorter ligated chains and longer protective chains. In this scenario, a repulsive potential of a steric nature (between the protective chains and the receptors) must be overcome to allow the adsorption of the nanoparticles on the receptor surface. This repulsion can be used to reduce the apparent ligand/receptor affinity and achieve an affinity conducive to super-selectivity (9, 15, 22). However, experimental evidence on the binding selectivity of BM is somehow limited.

In this work, a combination of experiments and analytical modeling are used to assess the efficiency of bimodal brush-functionalized gold nanoparticles (GNPs) in improving the adsorption selectivity (Fig. 1*A*). To this end, well-defined experimental systems

Author contributions: H.T.P., S.A.-U., J.L.C., and S.G. designed research; H.T.P., D.L., and S.A.-U. performed research; A.V.-B., S.A.-U., J.L.C., and S.G. contributed new reagents/analytic tools; H.T.P., D.L., S.A.-U., J.L.C., and S.G. analyzed data; and H.T.P., D.L., A.V.-B., S.A.-U., J.L.C., and S.G. wrote the paper.

The authors declare no competing interest.

This article is a PNAS Direct Submission.

[1]To whom correspondence may be addressed. Email: jeanne.leblond-chain@inserm.fr or suzanne.giasson@umontreal.ca.

This article contains supporting information online at https://www.pnas.org/lookup/suppl/doi:10.1073/pnas.2208377120/-/DCSupplemental.

Published January 11, 2023.

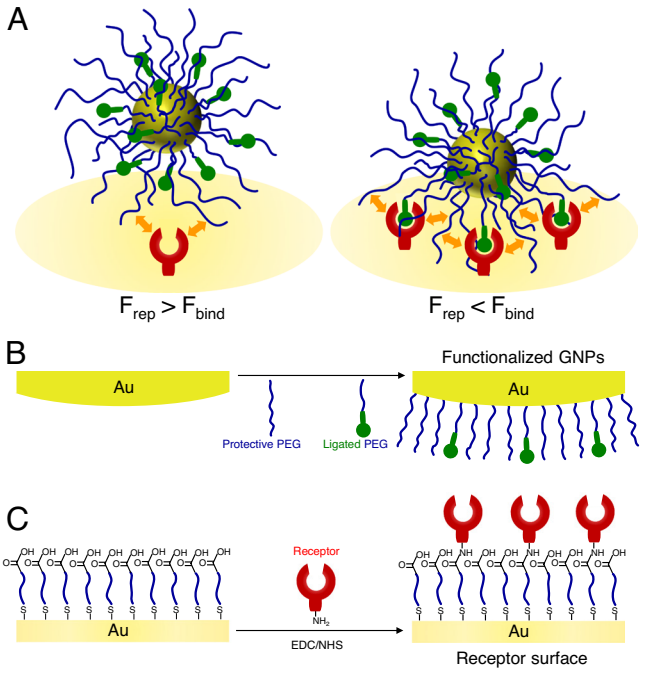

Fig. 1. (*A*) Schematic illustration of the main hypothesis of this work. Protective PEG chains offer steric repulsion (⟷) to modulate the ligand–receptor binding. Proper tuning of this repulsion enables the selective adsorption of nanoparticles to surface density of receptors. To model multivalent nanoparticle-cell surface interaction, we designed (*B*) bimodal brush-functionalized gold nanoparticles (GNPs) through thiolated-gold covalent bond and (*C*) receptor surfaces via peptide coupling.

biomimicking multivalent nanoparticle-cell surface adsorption are developed based on ligand–receptor interactions (Fig. 1 *B* and *C*). The extracellular domain of the mouse transferrin receptor (TfR, monomer, M_w = 78.3 KDa) is used as receptor since TfR is extensively studied for cancer targeting due to its overexpression on several cancer cells and its ability to trigger internalization of nanoparticles (23). The aptamer DW4 serves as a ligand to bind TfR, with moderate affinity (K_d = 190 nM) and specificity in TfR recognition (24). To quantify the GNPs adsorption on TfR surfaces, surface plasmon resonance technique (SPR) and atomic force microscopy (AFM) imaging were used. Furthermore, a analytical model describing GNPs adsorption from a solution to receptor-functionalized surfaces is built by adapting a previously reported model (15). Finally, the effect of the repulsive potential provided by the protective chains on the selectivity toward the receptor surface density is elucidated.

Results and Discussion

To model nanoparticle surfaces, spherical gold nanoparticles (GNPs) were surface-functionalized with a bimodal brush of protective polyethylene glycol (PEG) and ligand-bearing (ligated) PEG. The GNPs were selected because of the relative ease of surface functionalization (25) as well as their relevance to simulations using hard spheres (9). Citrate-capped gold nanoparticles (bare GNPs) were synthesized and characterized by TEM. The GNPs exhibited a spherical shape (circularity 0.9 ± 0.02) of 14.7 ± 0.8 nm diameter with a narrow size distribution (*SI Appendix*, Fig. S1 *A* and *B*). GNPs were then surface-functionalized with two end-functionalized polymers (SH-PEG and SH-PEG-DW4) through thiolated-gold bond (Au-S). The protective PEG is chosen to provide shielding properties and the PEG-DW4 to target the TfR (24). Since Au-S bond can undergo oxidation when exposed to light, air, or at elevated temperature (26), the stability of grafted PEG_{2K} on GNP was investigated in typical storage conditions. 67% of PEG_{2K} chains dissociated from GNPs surface after 20 d when stored at 4 °C in dark air atmosphere, while the number of PEG_{2K} chains was maintained for at least 20 d when stored at 4 °C in dark and under argon (*SI Appendix*, Table S1). Therefore, the functionalized GNPs were systematically stored in the latter conditions.

The extent of surface functionalization of the GNPs was indirectly assessed by measuring the particle size variation upon polymer grafting and through absorbance in UV-Vis. The size of all polymer-functionalized GNPs is significantly larger than that of the bare GNPs (*SI Appendix*, Fig. S1*C* and Table 1). Importantly, the polydispersity index (PDI) remained low (PDI < 0.25) in all samples, suggesting a relatively homogeneous functionalization. In addition, the polymer-coated GNPs induced a red shift (~4 to 7 nm) in the plasmon adsorption band due to the change in the dielectric constant at the nanoparticle surface (*SI Appendix*, Fig. S1*D* and Table 1).

As expressed in set of Eq. (*SI Appendix*, Eqs. **S9–S17**) (*SI Appendix*, section S1), the magnitude of the steric repulsion (βF_{rep}) is related to four main parameters of GNPs: the numbers of protective PEG and ligated PEG chains grafted on GNPs surface, N_{PEG} and $N_{PEG\text{-}DW4}$, respectively; the numbers of ethylene glycol units in protective PEG and ligated PEG chains, n_{PEG} and $n_{PEG\text{-}DW4}$, respectively. In the present study, the magnitude of βF_{rep} was tuned by three parameters N_{PEG}, n_{PEG}, and $n_{PEG\text{-}DW4}$ keeping $N_{PEG\text{-}DW4}$ constant. PEG of different M_w (2 and 5 KDa) and PEG-DW4 of different M_w (1 and 3 KDa) were used to modulate n_{PEG} and $n_{PEG\text{-}DW4}$. To keep $N_{PEG\text{-}DW4}$ constant while modulating N_{PEG}, the GNPs were functionalized with a fixed PEG-DW4-to-GNPs feeding ratio ($\Phi_{PEG\text{-}DW4/GNPs}$) of 58 chains/particle and an increasing PEG-to-GNPs feeding ratio ($\Phi_{PEG/GNPs}$) from 58 to 232 chains/particle. The total of $\Phi_{PEG\text{-}DW4/GNPs}$ and $\Phi_{PEG/GNPs}$ is much lower than that required for fully covering the surface [experimentally determined at ~2,500 chains/particle for GNPs diameter of 15 nm (27)]. Using such feeding ratio has shown to provide a good control of surface composition of the two chains (28). As shown in Table 1, GNPs were successfully functionalized with PEG and PEG-DW4 of various M_w and the parameter N_{PEG} was finely controlled by adjusting $\Phi_{PEG/GNPs}$ during functionalization. Increasing $\Phi_{PEG/GNPs}$ led to an increase in N_{PEG}. In addition, $N_{PEG\text{-}DW4}$ was nearly constant (~40 PEG-DW4 chains per particle). In summary, a library of polymer-functionalized GNPs with comparable physical characteristics (core size, PDI, λ_{SPR}, hydrodynamic diameter, $N_{PEG\text{-}DW4}$) was prepared, exhibiting different values of N_{PEG}, n_{PEG}, $n_{PEG\text{-}DW4}$, and βF_{rep}(Table 1).

To mimic cell membranes expressing various receptor surface densities, a set of self-assembled polymer monolayers (SAMs) functionalized with various amounts of transferrin receptors (TfR) were prepared. SAMs of SH-PEG_{2K}-COOH were formed on flat gold surfaces through S-Au bonds providing an available functional group (-COOH) for immobilizing TfR via peptide coupling (with the primary amine of lysine residues). The surface density of receptors (Γ_{TfR}) was tuned by the reaction time (between 1 and 60 min) and monitored in real time using SPR. Using this approach, Γ_{TfR} varies from 0.86 to 7.97 × 10^3 molecules/μm^2, depending on the coupling reaction time (Fig. 2*A* and *SI Appendix*, Table S2). The corresponding average number of receptors residing within the interacting area and available for the ligand binding is approximately between 0.2 and 3 (*SI Appendix*, Eq. **S22**).

To assess the binding interaction between DW4-free in solution and the surface-immobilized TfR, the dissociation constants (K_{bind}^{sol}) of TfR60 surface with either DW4 or with PEG_{3K}-DW4

Table 1. Characterization of GNPs functionalized with PEG/PEG-DW4 monolayers

Functionalized GNPs abbreviation*	PEG Mw (g/mol)	$\Phi_{PEG/GNPs}$ (chains/particle)	$N_{PEG\text{-}DW4}$ † (chains/particle)	N_{PEG} † (chains/particle)	βF_{rep} ‡ (per-receptor quantity)	DLS		λ_{SPR} UV-Vis (nm)
						D_h (nm)	PDI	
Bare GNPs		-	-	-		21 ± 2	0.11 ± 0.03	518.0
GNPs-5K	PEG: 5000	-	-	-		45 ± 2	0.12 ± 0.02	523.0
GNPs-3KDW4	PEG-DW4: 3000	-	-			43 ± 1	0.13 ± 0.02	522.4
GNPs-2K$_1$-3KDW4	PEG: 2000 PEG-DW4: 3000	58	37 ± 4	41 ± 2	0	38 ± 1	0.15 ± 0.02	523.5
GNPs-2K$_2$-3KDW4		116	38 ± 1	95 ± 12		40 ± 1	0.14 ± 0.03	524.0
GNPs-2K$_4$-3KDW4		232	36 ± 3	153 ± 2		39 ± 3	0.13 ± 0.02	524.0
GNPs-5K$_1$-3KDW4	PEG: 5000 PEG-DW4: 3000	58	39 ± 4	36 ± 2	0.052 ± 0.005	48 ± 1	0.18 ± 0.03	523.5
GNPs-5K$_2$-3KDW4		116	36 ± 3	69 ± 1	0.167 ± 0.003	52 ± 1	0.11 ± 0.02	524.5
GNPs-5K$_4$-3KDW4		232	40 ± 3	149 ± 8	0.608 ± 0.05	48 ± 2	0.12 ± 0.02	525.0
GNPs-2K$_1$-1KDW4	PEG: 2000 PEG-DW4: 1000	58	40 ± 2	41 ± 5	0.065 ± 0.015	31 ± 1	0.11 ± 0.02	522.0
GNPs-2K$_2$-1KDW4		116	43 ± 6	87 ± 2	0.279 ± 0.017	30 ± 1	0.09 ± 0.02	523.0
GNPs-2K$_4$-1KDW4		232	40 ± 4	165 ± 3	0.916 ± 0.035	32 ± 1	0.14 ± 0.03	522.0
GNPs-5K$_1$-1KDW4	PEG: 5000 PEG-DW4: 1000	58	38 ± 2	44 ± 1	0.759 ± 0.025	46 ± 3	0.17 ± 0.03	523.5
GNPs-5K$_2$-1KDW4		116	41 ± 1	80 ± 8	2.125 ± 0.350	43 ± 2	0.23 ± 0.02	523.5
GNPs-5K$_4$-1KDW4		232	40 ± 3	137 ± 7	5.179 ± 0.451	48 ± 2	0.23 ± 0.04	524.0

Hydrodynamic diameter (Dh), polydispersity index (PDI), plasmon adsorption band (λSPR). The error (±) is the standard deviation from three independent experiments.
*e.g., GNPs-2K$_1$-3KDW4 indicates GNP functionalized with PEG_{2K} and PEG_{3K}-DW4, with $\Phi_{PEG/GNPs}$ = 58 and $\Phi_{PEG\text{-}DW4/GNPs}$ = 58.
†$N_{PEG\text{-}DW4}$ and N_{PEG} are calculated from NMR, Fluorimetry and UV-vis results (*SI Appendix*, sections S.3.2, S.3.6, and Fig. S2).
‡βF_{rep} (per-receptor quantity) is calculated using set of equations (*SI Appendix*, Eqs. **S9**–**S17**) with N_R = 1 (*SI Appendix*, section S1).

were determined in aqueous solutions (PBS pH 7.4 buffer containing $MgCl_2$ 1 mM, PBS-M) using SPR. Both DW4 and PEG_{3K}-DW4 exhibited similar K_d values (106 ± 8 and 102 ± 5 nM, respectively, Fig. 2*B*) suggesting that tethering DW4 on a PEG chain does not affect the DW4/TfR interaction. These values are also consistent with the K_d reported in the literature for the same DW4/TfR couple in solution (190 nM) (24), confirming that immobilizing TfR on a substrate does not significantly impact the TfR/ligand binding. It is worth mentioning that when DW4 is tethered via a PEG chain, its interaction with TfR is expected to be reversible due to the configuration entropy (*SI Appendix*, section S.3.10). The theoretical dissociation constant when DW4 is grafted on GNPs surface k_{off}^{graft} is 7.4×10^4 s^{-1}, corresponding to a bond lifetime of 14 μs (*SI Appendix*, section S.3.10). This lifetime is much shorter than the experimental timescale (15 min). Therefore, we infer that bonds can re-arrange and are in equilibrium under our experimental conditions, in which super-selectivity has been shown to be possible.

To assess the specificity of DW4-bearing GNPs toward TfR surfaces, a series of controls was conducted using SPR to monitor the GNPs adsorption. Binding tests of GNPs/surfaces of different configurations in absence of TfR/DW4 couple (negative control) were compared with similar tests in the presence of TfR/DW4 couple (positive control) (Fig. 2*C*). As expected, a noticeable adsorption ($\Delta\lambda_{SPR}$ of 4.2 nm) was observed only when TfR-functionalized surfaces (TfR60) were exposed to DW4-bearing GNPs. Importantly, no adsorption (no $\Delta\lambda_{SPR}$) was detected when PEG-functionalized surfaces were exposed to DW4-free or DW4-bearing GNPs, neither when TfR-functionalized surfaces were exposed to DW4-free GNPs, confirming the absence of GNPs adsorption in the absence of the TfR/DW4 couple. These observations demonstrate that the adsorption of DW4-bearing GNPs on the TfR-functionalized surfaces is driven solely by the specific TfR/DW4 interactions. Similar experiments performed using AFM imaging to detect the adsorbed GNPs support this conclusion (*SI Appendix*, Fig. S5).

To quantify the selectivity of nanoparticles toward the receptor surface density, the selectivity parameter α introduced by Martinez–Veracoechea and Frenkel (7) was used:

$$\alpha \equiv \frac{d \ln \tau_{NP}}{d \ln \tau_{TfR}}. \quad [1]$$

The parameter α refers to the relative change in the number of adsorbed nanoparticles [Γ_{NP}, number of particles per μm^2 (NP/μm^2)] in response to the variation in the number of receptors on a cell (Γ_{TfR}, molecule/μm^2). A system is considered as highly selective or super-selective when α > 1 (7). When the parameter α

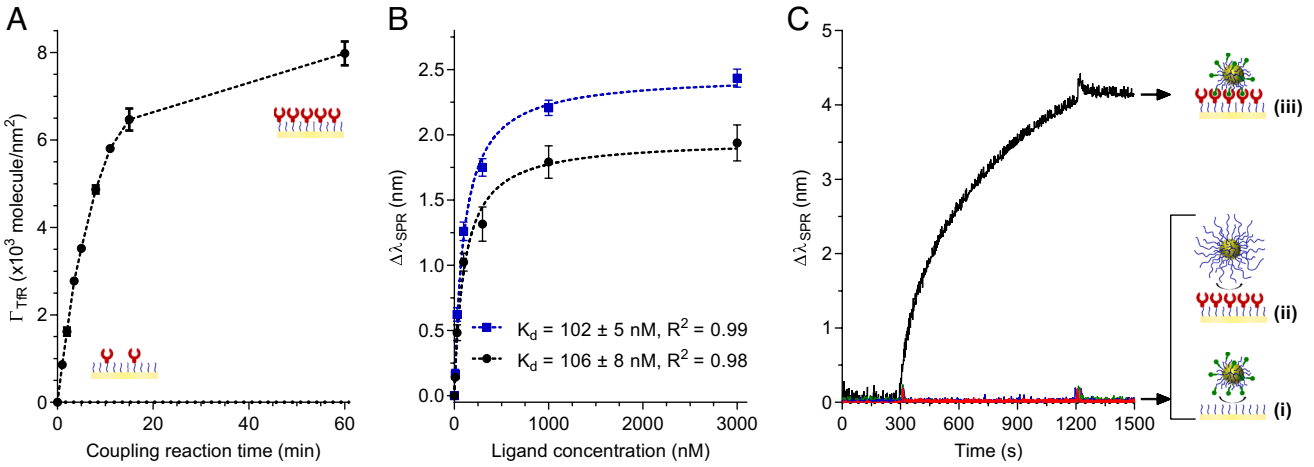

Fig. 2. Characterization of transferrin receptor (TfR)-functionalized surfaces. (*A*) Receptor surface density (Γ_{TfR}) at different coupling reaction times. The receptor density (Γ_{TfR}) was then calculated from λ_{SPR} shift ($\Delta\lambda_{SPR}$) using the Jung et al.'s equation (29) (*SI Appendix*, section S.3.7). The dash black line is a guide for the eyes, the SPR raw data are present in *SI Appendix*, Table S2. (*B*) Determination of the dissociation equilibrium constant (K_d) between TfR and DW4 aptamer ligand using SPR-binding analysis. λ_{SPR} shifts (nm) at equilibrium are plotted versus DW4 (-■-) or DW4-PEG3K (-●-) concentration. Fitting curves (blue and black dashed lines) and K_d values were obtained from fitting the experimental data to binding saturation (one site-specific binding) model using Graphpad prism software. Error bars represent the standard deviation of the means of SPR measurements of three sensing areas on three independent samples. SPR sensorgrams of TfR60 surface exposed to increasing concentrations of DW4 or DW4-PEG3K are reported in *SI Appendix*, Fig. S4. (*C*) SPR sensorgrams of PEG-functionalized surfaces exposed to GNPs-2K-3KDW4 (red), to GNPs-5K-3KDW4 (blue) (i); TfR60 surfaces exposed to GNPs-2K (green), to GNPs-5K (violet) (ii); and TfR60 surfaces exposed to GNPs-2K-3KDW4 (black) (iii).

reaches at maximum value (α_{max}), the corresponding receptor surface density is defined as the onset density (Γ_{onset}). It is worth mentioning that around Γ_{onset}, a slight variation in Γ_{TfR} leads to a supralinear change in Γ_{NP} (15). The adsorption of GNPs in response to the variation in Γ_{TfR} was investigated using SPR for two formulations: GNPs-5K$_4$-3KDW4 and GNPs-2K$_4$-3KDW4 as representative for bimodal monolayers with unfunctional PEG that are longer and shorter, respectively, than the ligated PEG. The GNPs adsorption (Γ_{NP}) and the corresponding selectivity (α) as a function of Γ_{TfR} are illustrated in Fig. 3 and *SI Appendix*, Fig. S6, respectively. Γ_{NP} of both GNPs formulations is responsive to Γ_{TfR} and two regimes can be identified. At $\Gamma_{TfR} < \Gamma_{onset}$, the Γ_{NP} is negligible and does not vary with Γ_{TfR}. However, it increases greater than linearly (supralinearly) above Γ_{onset}. This observed behavior demonstrates that both bimodal systems exhibit a certain degree of super-selectivity, thanks to the multivalency effect (7, 8). The GNPs-5K$_4$-3KDW4 exhibits a lower adsorption but a higher selectivity (higher Γ_{onset} and α_{max}) compared to GNPs-2K$_4$-3KDW4. The only variable between these two GNPs formulations is the M_w (length) of protective PEG (5 kDa versus 2 kDa). Hence, the enhanced selectivity is likely due to the presence of longer protective PEG, in a good agreement with Monte Carlo simulation (9, 22) and recent theoretical prediction (15). The "near-plateau" region observed for both systems is likely due to the fact that at some point, a maximum number of adsrobed particles is reached because of excluded volume effects. From Fig. 3, we also notice that the adsorption curve for GNPs-5K$_4$-3KDW4 saturates at a lower level than that for GNPs-2K$_4$-3KDW4. Firstly, the excluded volume of PEG brush on GNPs-5K$_4$-3KDW4 is expected to be larger than that on GNPs-2K4-3KDW4 because of the larger shell of protective PEG chains (PEG_{5K} versus PEG_{3K}) (30), leading to a lower maximum number of particles adsorbed. Secondly, considering the adsorption of multivalent nanoparticles covered with a protective polymer brush (as our GNPs), there is always a maximum (sometimes mistaken for a plateau) that can be reached; afterward, the adsorption is expected to decrease with increasing receptor surface densities due to the steric repulsion. When the protective polymer is longer (in our case, PEG_{5K} versus PEG_{3K}), the repulsion is stronger, and subsequently, the maximum adsorption is observed at a lower level and arises at lower surface density of receptor (19). The SPR sensorgrams of GNPs adsorption are shown in *SI Appendix*, Fig. S7. Adsorbed GNPs do not desorb after rinsing with buffer. The observed phenomenon is likely due to the multivalent nature of GNPs adsorption. For multivalent nanoparticles to be unbound, all interacting ligands must be unbound at the same time and must also remain so for a timescale larger than the time it takes to diffuse away from the receptor surface. The interacting ligands are all those residing within the interacting area and being available for receptor binding, which

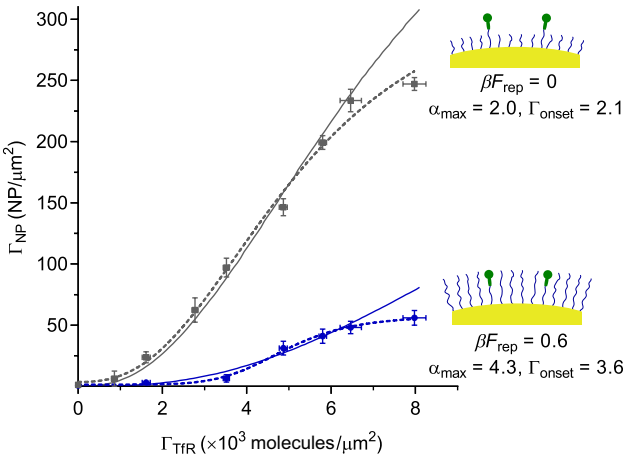

Fig. 3. GNPs adsorption Γ_{NP}, measured by SPR (see *SI Appendix*, section S.3.8 for details on Γ_{NP} determination from SPR results and see *SI Appendix*, Fig. S7 for SPR sensorgrams), as a function of Γ_{TfR} for GNPs-2K$_4$-3KDW4 (■) and GNPs-5K4-3KDW4 (●), error bars represent the standard deviation of the means of SPR measurements of three sensing areas on three independent samples. The empirical fitting curves for GNPs-2K4-3KDW4 (— — —) and for GNPs-5K4-3KDW4 (— — —) are sigmoidal curves obtained by using Graphpad prism (R^2 are 0.99 and 0.95, respectively). The fitted theoretical curves for GNPs-2K$_4$-3KDW4 (——) and GNPs-5K4-3KDW4 (——) are generated by the theory, as described in *SI Appendix*, section S1, the value of the two fitting constants are C = 5/2 and $\beta\Delta G_{conf}$ = 13.5. The selectivity parameters α_{max} and Γ_{onset} are determined from the plot of α versus Γ_{TfR} (*SI Appendix*, Fig. S6).

is approximatively 13 and 18 for GNPs-2K_4-3KDW4 and GNPs-5K_4-3KDW4, respectively (*SI Appendix*, Eq. **S20**). $t = L^2 / D$ (Strokes–Einstein law), where L being the binding distance (*SI Appendix*, Eqs. **S18** and **S19**), D is the diffusion coefficient of GNPs. The calculated t is 0.06 and 0.01 μs for GNPs-2K_4-3KDW4 and GNPs-5K_4-3KDW4, respectively, which is 233 and 1,400 times shorter than the lifetime of the individual ligand–receptor bond (*SI Appendix*, section S.3.10), leading to irreversible adsorption of GNPs even when the single bonds are instead reversible. This is a fact that has been experimentally confirmed for other multivalent systems, *e.g.,* the work of Dubacheva et al. (13, 18) where irreversible multivalent adsorption is reported at timescales where the single bond was reversible.

To rationalize the experimental selectivity of GNPs, a predictive model for the adsorption behavior of the nanoparticles was developed by adapting a model previously described (15, 19), which is an extension of Martinez–Veracoechea and Frenkel model (7). This model is described in detail in Materials and Methods. The solid lines in Fig. 3 are the result of a fit to the experimental data (the adsorption curves of GNPs-5K_4-3KDW4 and GNPs-2K_4-3KDW4) with the model using two adjustable parameters: the dimensionless scaling factor C and the configurational bond penalty $\beta\Delta G_{conf}$. This analytical model is based on a simplified coarse-grained description and is not expected to capture all details of the experimental systems; however, semi-quantitative, or at least qualitative agreement can be expected. For example, the model ignores allosteric cooperative effects (31) by assuming that individual ligand–receptor bonds form independently. It also excludes the effect of ligand size on the repulsion of the polymer brush. Nevertheless, Fig. 3 shows a good agreement between the experimental results and the modeling predictions. In particular, the theoretical model quantitatively reproduces the drop in GNPs adsorption of GNPs-5K_4-3KDW4, compared to GNPs-2K_4-3KDW4, and qualitatively captures the increase in selectivity of GNPs adsorption (higher Γ_{onset} and α_{max}) of GNPs-5K_4-3KDW4, compared to GNPs-2K_4-3KDW4 (*SI Appendix*, Fig. S6). In addition, the obtained values of the two fitting parameters C = 5/2, and $\beta\Delta G_{conf}$ = 13.5 are within the expected order of magnitude. For example, $\beta\Delta G_{conf}$ of ethylene glycol linker in DNA-coated colloids is found to be ~12.6 to 15.7 (32). The agreement between the experimental and theoretical results provides additional evidence on the selectivity enhancement of the longer protective PEG. The long protective chains provide a repulsive barrier that nanoparticles must overcome to interact with receptor surfaces. A larger Γ_{onset} is required to provide a sufficient attraction between the GNPs and the receptor to overcompensate this steric barrier, hence favoring nanoparticle adsorption. Above the Γ_{onset}, the attraction generated by the formation of ligand–receptor bonds increases supralinearly with the receptor surface density Γ_{TfR}. Consequently, the nanoparticle adsorption is highly selective to receptor surface density.

To further investigate the effect of the repulsive potential on the selectivity, the adsorption of various GNPs, exhibiting different values of N_{PEG}, n_{PEG}, $n_{PEG\text{-}DW4}$, and βF_{rep} (Table 1), was measured for two representative TfR surfaces: one with low coverage (TfR5, $\Gamma_{TfR} = 3.52 \times 10^3$ molecules/nm^2) and the other with high coverage (TfR60, $\Gamma_{TfR} = 7.98 \times 10^3$ molecules/nm^2) (Fig. 2*A* and *SI Appendix*, Table S2). The GNPs adsorption data are shown in *SI Appendix*, Table S3. A selectivity parameter $\alpha_{TfR60\text{-}TfR5}$ was calculated based on Eq. **1** using two Γ_{TfR} values (3.52×10^3 and 7.98×10^3 molecules/nm^2). $\alpha_{TfR60\text{-}TfR5}$ represents the ability of GNPs to selectively discriminate the TfR60 surface from the TfR5 one. The parameter $\alpha_{TfR60\text{-}TfR5}$ was plotted as a function of the number of protective PEG chains on GNPs surface N_{PEG}, the number of ethylene glycol units in protective PEG n_{PEG} (Fig. 4). Fig. 4*A* shows that an increase in N_{PEG} leads to an increase in $\alpha_{TfR60\text{-}TfR5}$. Fig. 4*B* shows that increasing n_{PEG} from 46 to 114 leads to an increase in $\alpha_{TfR60\text{-}TfR5}$. Note that increasing N_{PEG} or n_{PEG} theoretically leads to an increase in the magnitude of the repulsive potential βF_{rep} (*SI Appendix*, Eqs. **S9**–**S17** and Fig. S9). The plot of $\alpha_{TfR60\text{-}TfR5}$ versus βF_{rep} (*SI Appendix*, Fig. S10) shows that $\alpha_{TfR60\text{-}TfR5}$ increases with increasing βF_{rep}. This trend is more pronounced for longer ligated chains (PEG_{3K}-DW4 versus PEG_{1K}-DW4). As described in the theoretical model, the length of ligated chains affects the adsorption energy, the longer the chain, the stronger the attraction. When the ligated chains are long, the growth of the combinatorial entropy with receptor surface density is strong enough to overcome βF_{rep}, ensuring adsorption to receptor-functionalized surfaces of high coverage. In summary, the results confirm that it is experimentally possible to tune the selectivity of GNPs (TfR60 over TfR5) by adjusting the ligated chain length and the magnitude of βF_{rep} (by changing N_{PEG}, n_{PEG}). The

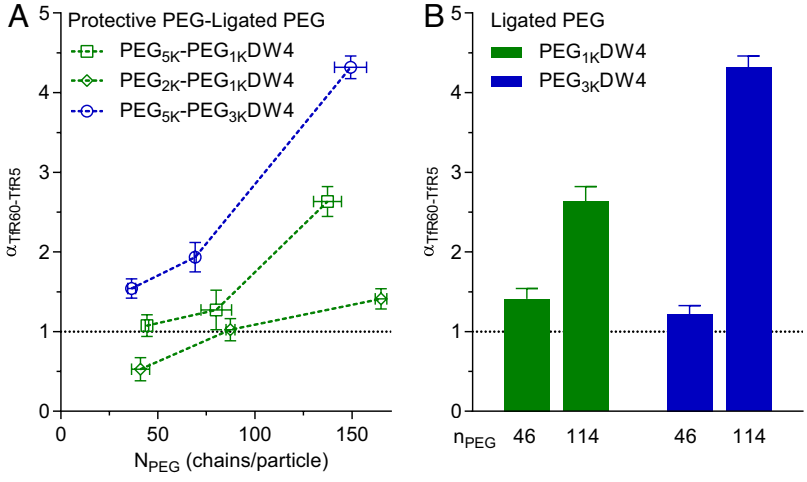

Fig. 4. Effect of the number of protective PEG chains on GNPs surface N_{PEG} (*A*), the number of ethylene glycol units in protective PEG n_{PEG} (*B*) on the parameter $\alpha_{TfR60\text{-}TfR5}$. The number of adsorbed GNPs was measured by AFM (*SI Appendix*, Tables S3 and S4). Error bars represent the standard deviation of the means of AFM measurements of three different areas on three independent samples. A comparison between SPR and AFM data shows no significant difference (*SI Appendix*, Fig. S8).

selectivity increases with an increase in βF_{rep} and the longer the ligated chains, the stronger the βF_{rep} effect.

It is relevant to mention some limitations of the present experimental models. The cell membrane was modeled using TfR-immobilized SAMs of PEG whereas natural cell membranes are known to display on their surface not only receptors but also some other polymers such as glycocalyx (33). Like protective chains, the glycocalyx chains can provide additional repulsive forces between the nanoparticles and the cell surface (15, 19). In addition, the elasticity and the curvature effect of the cells (34) are not taken into account in the cell membrane model. For a deformable surface, the interface between the nanoparticles and the receptor-functionalized surfaces can be convex-on-concave or convex-on-convex, depending on the overall interactions between the nanoparticles and the receptor surfaces. For convex-on-concave contact, the numbers of interacting ligand and receptors (N_L and N_R) will be larger than that for convex-on-flat contact and the reverse scenario for convex-on-convex contact. Consequently, both attractive and repulsive contributions will change in the same direction as that for a change in N_L and/or N_R. To address this point, experimental measurements of nanoparticle adsorption on cells, receptor-functionalized giant synthetic lipid vesicles, or detailed theoretical modeling (35) would be required.

Conclusion

In conclusion, we have developed highly specific and tunable experimental systems modeling multivalent nanoparticle-cell surface adsorption. Using these systems in combination with theoretical modeling, an unprecedented detailed and systematic experimental evidence on the selectivity of bimodal monolayer-functionalized nanoparticles toward the receptor surface density is demonstrated. This study confirms that a bimodal monolayer with longer protective chains provides a better selectivity (by increasing both the adsorption onset and the selectivity parameter α), compared to the one with shorter protective chains as previously suggested by simulation and theoretical studies. A relationship between the repulsion due to protective chains and the selectivity was established and provides a practical guide to design nanoparticles for targeting specific receptor surface density. The presented approach is useful for the development of nanoparticle-based drug delivery systems or other applications such as cell sorting, detection of receptor surface density, and selective purification devices.

Materials and Methods

A detailed description of the theoretical model, materials and experimental methods is presented in SI. DNA syntheses were performed using standard phosphoramidite chemistry with a DNA/RNA synthesizer H-6 from K&A Laborgeraete. See *SI Appendix* or ref. 24 for DW4 sequence. Bare GNPs were synthetized by a modified Frens method (36). Flat gold surfaces for TfR surface preparation were prepared by gold coating on silicon wafer or SPR sensors (dove BK7 prisms) using a Cressington 308R sputter coater. All GNPs adsorption experiments were carried out in PBS (1× pH 7.4) buffer containing $MgCl_2$ 1 mM (PBS-M) at 25 °C. In these conditions, MD simulation and HPLC analysis show that DW4 adopts folded structures and the active one represents approximatively 95 mol% (*SI Appendix*, Fig. S11 and ref. 24). The GNPs concentration was fixed at 100 pM since GNPs were shown to form clusters at larger GNPs concentration (500 pM) (*SI Appendix*, Fig. S12 and section S.3.3). AFM imaging by a Multimode microscope equipped with a Nanoscope V extended controller (*SI Appendix*, section S.3.5 and Fig. S13 for the identification of adsorbed GNPs on AFM height images). A comparison between AFM and scanning electron microscopy results showed no significant difference in GNPs adsorption (*SI Appendix*, Fig. S14). SPR analysis by a portable 4-channel SPR instrument (37).

Data, Materials, and Software Availability. All study data are included in the article and/or *SI Appendix*.

ACKNOWLEDGMENTS. We would like to acknowledge Prof. Jean-Francois Masson for the use of his SPR device and useful discussions. Financial supports from the Natural Sciences and Engineering Research Council of Canada (NSERC) and the Fonds de recherche du Québec–Nature et technologies (FRQNT) are acknowledged for Discovery (RGPIN-2016-06766) and Research Tools and Instrument grants. Financial supports from the Université de Montréal and the Quebec Centre for Advanced Materials (QCAM) are also acknowledged. A.V.-B. is Canada Research Chair in Bioengineering and Bionanotechnology, Tier II and acknowledges a Discovery Grants (RGPIN-2020-06975) from NSERC. D.L. acknowledges a 3rd cycle scholarship from the FRQNT.

Author affiliations: [a]Faculty of Pharmacy, University of Montreal, Montreal H3C 3J7, QC, Canada; [b]Department of Chemistry, University of Montreal, Montreal H3C 3J7, QC, Canada; [c]Department of Materials, Imperial College London, London SW7 2AZ, UK; and [d]University of Bordeaux, CNRS, UMR 5320, INSERM, Bordeaux U1212, F-33000, France

1. M. J. Mitchell *et al.*, Engineering precision nanoparticles for drug delivery. *Nat. Rev. Drug. Discovery* **20**, 101–124 (2021).
2. L. Woythe, N. B. Tito, L. Albertazzi, A quantitative view on multivalent nanomedicine targeting. *Adv. Drug. Delivery Rev.* **169**, 1–21 (2021).
3. M. Mammen, S.-K. Choi, G. M. Whitesides, Polyvalent interactions in biological systems: Implications for design and use of multivalent ligands and inhibitors. *Angew. Chem. Int. Ed.* **37**, 2754–2794 (1998).
4. L. L. Kiessling, A. C. Lamanna, "Multivalency in biological systems" in *Chemical Probes in Biology*, M. P. Schneider, Ed. (Springer, Netherlands, 2003), pp. 345–357.
5. A. Joshi, D. Vance, P. Rai, A. Thiyagarajan, R. S. Kane, The design of polyvalent therapeutics. *Chem. A. Eur. J.* **14**, 7738–7747 (2008).
6. P. Li *et al.*, Phase transitions in the assembly of multivalent signalling proteins. *Nature* **483**, 336–340 (2012).
7. F. J. Martinez-Veracoechea, D. Frenkel, Designing super selectivity in multivalent nano-particle binding. *Proc. Natl. Acad. Sci. U.S.A.* **108**, 10963–10968 (2011).
8. P. I. Kitov, D. R. Bundle, On the nature of the multivalency effect: A thermodynamic model. *J. Am. Chem. Soc.* **125**, 16271–16284 (2003).
9. S. Wang, E. E. Dormidontova, Selectivity of ligand-receptor interactions between nanoparticle and cell surfaces. *Phys. Rev. Lett.* **109**, 238102 (2012).
10. N. A. Licata, A. V. Tkachenko, Kinetic limitations of cooperativity-based drug delivery systems. *Phys. Rev. Lett.* **100**, 158102 (2008).
11. M. R. W. Scheepers, L. J. van IJzendoorn, M. W. J. Prins, Multivalent weak interactions enhance selectivity of interparticle binding. *Proc. Natl. Acad. Sci. U.S.A.* **117**, 22690–22697 (2020).
12. E. Magdalena Estirado, M. A. Aleman Garcia, J. Schill, L. Brunsveld, Multivalent ultrasensitive interfacing of supramolecular 1D nanoplatforms. *J. Am. Chem. Soc.* **141**, 18030–18037 (2019).
13. G. V. Dubacheva *et al.*, Superselective targeting using multivalent polymers. *J. Am. Chem. Soc.* **136**, 1722–1725 (2014).
14. C. B. Carlson, P. Mowery, R. M. Owen, E. C. Dykhuizen, L. L. Kiessling, Selective tumor cell targeting using low-affinity, multivalent interactions. *ACS Chem. Biol.* **2**, 119–127 (2007).
15. X. Tian, S. Angioletti-Uberti, G. Battaglia, On the design of precision nanomedicines. *Sci. Adv.* **6**, eaat0919 (2020).
16. S. Wang, E. E. Dormidontova, Nanoparticle design optimization for enhanced targeting: Monte Carlo simulations. *Biomacromolecules* **11**, 1785–1795 (2010).
17. S. Wang, E. E. Dormidontova, Nanoparticle targeting using multivalent ligands: Computer modeling. *Soft Matter.* **7**, 4435–4445 (2011).
18. G. V. Dubacheva, T. Curk, R. Auzély-Velty, D. Frenkel, R. P. Richter, Designing multivalent probes for tunable superselective targeting. *Proc. Natl. Acad. Sci. U.S.A.* **112**, 5579–5584 (2015).
19. M. Liu *et al.*, Combinatorial entropy behaviour leads to range selective binding in ligand-receptor interactions. *Nat. Commun.* **11**, 4836 (2020).
20. L. Albertazzi *et al.*, Spatiotemporal control and superselectivity in supramolecular polymers using multivalency. *Proc. Natl. Acad. Sci. U.S.A.* **110**, 12203–12208 (2013).
21. S. Angioletti-Uberti, Theory, simulations and the design of functionalized nanoparticles for biomedical applications: A soft matter perspective. *npj Comput. Mater.* **3**, 48 (2017).
22. T. Curk, N. B. Tito, First-order "hyper-selective" binding transition of multivalent particles under force. *J. Phys. Condens. Matter* **32**, 214002 (2020).
23. T. R. Daniels, The transferrin receptor and the targeted delivery of therapeutic agents against cancer. *Biochim. Biophys. Acta (BBA) - Gen. Subjects* **1820**, 291–317 (2012).
24. D. Porciani *et al.*, Two interconvertible folds modulate the activity of a DNA aptamer against transferrin receptor. *Mol Ther Nucleic Acids.* **3**, e144 (2014).
25. W. Chen, S. Zhang, Y. Yu, H. Zhang, Q. He, Structural-engineering rationales of gold nanoparticles for cancer theranostics. *Adv. Mater.* **28**, 8567–8585 (2016).
26. L. Srisombat, A. C. Jamison, T. R. Lee, Stability: A key issue for self-assembled monolayers on gold as thin-film coatings and nanoparticle protectants. *Colloids Surf. A* **390**, 1–19 (2011).
27. C. D. Walkey, J. B. Olsen, H. Guo, A. Emili, W. C. W. Chan, Nanoparticle size and surface chemistry determine serum protein adsorption and macrophage uptake. *J. Am. Chem. Soc.* **134**, 2139–2147 (2012).
28. A. Stewart, S. Zheng, M. R. McCourt, S. E. J. Bell, Controlling assembly of mixed thiol monolayers on silver nanoparticles to tune their surface properties. *ACS Nano* **6**, 3718–3726 (2012).

29. L. S. Jung, C. T. Campbell, T. M. Chinowsky, M. N. Mar, S. S. Yee, Quantitative interpretation of the response of surface plasmon resonance sensors to adsorbed films. *Langmuir* **14**, 5636–5648 (1998).
30. A. Zaki, N. Dave, J. Liu, Amplifying the macromolecular crowding effect using nanoparticles. *J. Am. Chem. Soc.* **134**, 35–38 (2012).
31. C. A. Hunter, H. L. Anderson, What is cooperativity? *Angew. Chem. Int. Ed.* **48**, 7488–7499 (2009).
32. M. E. Leunissen, R. Dreyfus, R. Sha, N. C. Seeman, P. M. Chaikin, Quantitative study of the association thermodynamics and kinetics of DNA-coated particles for different functionalization schemes. *J. Am. Chem. Soc.* **132**, 1903–1913 (2010).
33. J.C.-H. Kuo, J. G. Gandhi, R. N. Zia, M. J. Paszek, Physical biology of the cancer cell glycocalyx. *Nat. Phys.* **14**, 658–669 (2018).
34. J. Zimmerberg, M. M. Kozlov, How proteins produce cellular membrane curvature. *Nat. Rev. Mol. Cell Biol.* **7**, 9–19 (2006).
35. B. M. Mognetti, P. Cicuta, L. Di Michele, Programmable interactions with biomimetic DNA linkers at fluid membranes and interfaces. *Rep. Prog. Phys.* **82**, 116601 (2019).
36. X. Ji *et al.*, Size control of gold nanocrystals in citrate reduction: The third role of citrate. *J. Am. Chem. Soc.* **129**, 13939–13948 (2007).
37. S. S. Zhao *et al.*, Miniature multi-channel SPR instrument for methotrexate monitoring in clinical samples. *Biosens. Bioelectron.* **64**, 664–670 (2015).